Numerical discretization of energy-transport models for semiconductors with non-parabolic band structure

Pierre Degond
Université P. Sabatier Toulouse 3, UFR MIG, 118 route de Narbonne, F – 31062 Toulouse Cedex, France, e-mail: degond@mip.ups-tlse.fr

Ansgar Jüngel
Fachbereich Mathematik, Technische Universität Berlin, Straße des 17. Juni 136, D – 10623 Berlin, Germany, e-mail: jungel@math.tu-berlin.de

Paola Pietra
Istituto di Analisi Numerica, C.N.R., Via Abbiategrasso 209, I – 27100 Pavia, Italy, e-mail: pietra@dragon.ian.pv.cnr.it

Abstract

The energy-transport models describe the flow of electrons through a semiconductor crystal, influenced by diffusive, electrical and thermal effects. They consist of the continuity equations for the mass and the energy, coupled to Poisson's equation for the electric potential. These models can be derived from the semiconductor Boltzmann equation.

This paper consists of two parts. The first part concerns with the modelling of the energy-transport system. The diffusion coefficients and the energy relaxation term are computed in terms of the electron density and temperature, under the assumptions of non-degenerate statistics and non-parabolic band diagrams. The equations can be rewritten in a drift-diffusion formulation which is used for the numerical discretization.

In the second part, the stationary energy-transport equations are discretized using the exponential fitting mixed finite element method in one space dimension. Numerical simulations of a ballistic diode are performed.

Keywords. Mixed finite-element method, exponential fitting, non-parabolic band structure, semiconductors.

1991 Mathematics Subject Classification. 65N30, 65C20, 78A35.

Acknowledgments. The first and second author acknowledge support from the DAAD-PROCOPE Program, the second and third author are partly supported by the DAAD-Vigoni Program and by the Program on *Charged Particles Kinetics* at the Erwin Schrödinder Institute, Vienna. All three authors acknowledge support from the TMR Project "Asymptotic Methods in Kinetic Theory", grant number ERB-FMBX-CT97-0157. The second author acknowledge support from the Gerhard-Hess Program of the Deutsche Forschungsgemeinschaft.

1 Introduction

Semiconductor devices can be simulated by means of the semiconductor Boltzmann equation, which is usually numerically solved by employing the Monte-Carlo method. However, this method is too costly and time consuming to model real problems in semiconductor applications. Acceptable accuracy can be reached by solving macroscopic semiconductor models derived from the Boltzmann equation. The simplest models are drift-diffusion models which consist of the mass continuity equation for the charge carriers and a definition for the particle current density (see, e.g., [24]). These models, however, are not accurate enough for submicron device modeling, owing to the rapidly changing fields and temperature effects.

The energy-transport equations consist of the conservation laws of mass and energy, together with constitutive relations for the particle and energy currents, and are able to model temperature effects in submicron devices. Since the energy-transport equations are of parabolic type, the numerical solution needs less effort than the hydrodynamic models. Moreover, the energy-transport equations can be written in a drift-diffusion formulation, therefore the numerical effort is comparable to the drift-diffusion models.

In this paper a numerical scheme for energy-transport models is presented and numerical results for a one-dimensional ballistic diode are given. The originality of this paper consists of three facts: Firstly, we compute explicitly, for rather general band diagrams, diffusion coefficients and the energy relaxation term in terms of the electron density and temperature. For non-parabolic bands in the sense of Kane, the coefficients can be computed analytically. The resulting model is *completely* derived from the Boltzmann equation. Secondly, we show that *any* energy-transport model, derived from the Boltzmann equation via the "spherical harmonic expansion" (SHE) model under rather weak assumptions on the semiconductor band structure, allows a drift-diffusion formulation. Finally, based on the drift-diffusion formulation, we discretize and solve the equations by means of mixed finite elements and point out the differences of various models used in the physical literature.

The first part of this paper is concerned with the computation of the diffusion coefficients and the energy relaxation term, assuming general non-parabolic band diagrams and Boltzmann statistics (Section 2). In [5] the energy-transport equations are derived from the semiconductor Boltzmann equation by means of the Hilbert expansion method. First, the SHE model is obtained in the diffusion limit, under the assumption of dominant elastic scattering. Then, through a diffusion approximation, respectively making electron-electron or phonon scattering large, the energy-transport equations are derived from the SHE model. The stationary energy-transport model reads as follows:

$$
\begin{aligned}
-\mathrm{div}\, J_1 &= 0, && (1)\\
-\mathrm{div}\, J_2 &= -J_1 \cdot \nabla V + W(n,T), && (2)\\
J_1 &= L_{11}\Big(\nabla \frac{q\mu}{k_B T} - \frac{q\nabla V}{k_B T}\Big) + L_{12}\nabla\Big(-\frac{1}{k_B T}\Big), && (3)\\
qJ_2 &= L_{21}\Big(\nabla \frac{q\mu}{k_B T} - \frac{q\nabla V}{k_B T}\Big) + L_{22}\nabla\Big(-\frac{1}{k_B T}\Big), && (4)\\
\varepsilon_s \Delta V &= q(n-C). && (5)
\end{aligned}
$$

The variables are the chemical potential μ, the electron temperature T, and the electric potential V. Furthermore, J_1, J_2 are the particle and energy current densities, respectively.

The physical constants are the elementary charge q, the Boltzmann constant k_B, and the semiconductor permittivity ε_s. The electron density n depends on μ and T. For instance, for Boltzmann statistics and parabolic bands, the relation $n = N_i T^{3/2} \exp(q\mu/k_B T)$ with $N_i > 0$ holds. The space dependent function $C = C(x)$ is the doping profile, $L_{ij} = L_{ij}(n,T)$ are the diffusion coefficients, and $W = W(n,T)$ is the energy relaxation term. These equations hold in the (bounded) semiconductor domain Ω, and they have to be complemented with mixed Dirichlet-Neumann boundary conditions

$$\begin{aligned} n = n_D, \quad T = T_D, \quad V = V_D \qquad & \text{on } \Gamma_D, \\ J_1 \cdot \nu = J_2 \cdot \nu = \nabla V \cdot \nu = 0 \qquad & \text{on } \Gamma_N, \end{aligned}$$

modeling the Ohmic contacts Γ_D and the insulating boundary parts Γ_N. Then, $\partial\Omega = \Gamma_D \cup \Gamma_N$ and $\Gamma_D \cap \Gamma_N = \emptyset$ must be satisfied. The exterior normal unit vector on $\partial\Omega$ is denoted by ν.

The mathematical analysis of the equations (1)-(5) has been studied recently in [11, 12, 13, 17] (also see [1, 15]). The existence and uniqueness of solutions to both the stationary and the time-dependent equations have been proved. In the physical literature, the energy-transport equations are investigated numerically since several years [2, 9, 10, 21, 30, 31, 32], using parabolic band structure and Boltzmann statistics. Non-parabolic and non-Maxwellian distribution effects are discussed in [9, 31], but no comparisons of energy-transport models with parabolic and non-parabolic band diagrams have been performed.

In Section 2 we compute the diffusion coefficients L_{ij}, the electron density n, the internal energy E, and the energy relaxation term W in terms of μ and T. We assume that the energy-band diagram of the semiconductor crystal is spherically symmetric and monotone in the modulus of the wave vector $\vec{k}$, that non-degenerate Boltzmann statistics can be used and that a momentum relaxation time τ can be defined by $\tau(\varepsilon) \sim \varepsilon^{-\beta} N(\varepsilon)^{-1}$, where ε is the energy, $N(\varepsilon)$ denotes the density of states, and $\beta > -2$ is a parameter. Then, using the general formulas for the coefficients and densities from [5], we get more explicit expressions than those of [5], involving the energy-band function $\varepsilon(\vec{k})$ and depending on the temperature T (see Section 2.2).

Furthermore, we get *analytical* expressions under the additional assumption of non-parabolic bands in the sense of Kane [19]:

$$\varepsilon(1 + \alpha\varepsilon) = \frac{\hbar^2}{2m_0}|\vec{k}|^2,$$

where $\hbar$ is the reduced Planck constant, m_0 the effective electron mass, and $\alpha > 0$ the non-parabolicity parameter.

The second part of this paper is concerned with the numerical discretization of the energy-transport equations (Section 3). An important observation is that the current densities can be written in a drift-diffusion formulation of the form

$$J_i = \nabla g_i(n,T) - g_i(n,T)\frac{\nabla V}{T}, \quad i = 1, 2, \tag{6}$$

where g_1 and g_2 are non-linear functions of n and T. This formulation is valid for any current densities coming from a SHE model, involving Boltzmann statistics (see Section 2.3). It is the basis for our numerical discretization. For constant temperature, the expression (6) reduces to the standard drift-diffusion current definition.

The continuity equations (6) are discretized with a variant of the mixed exponential fitting scheme, which have been developed and studied in [6, 7, 8, 23] for the linear drift-diffusion equations and extended to a nonlinear driftdiffusion model in [18]. The most important features of these schemes are the current conservation (the current is introduced as independent variable and continuity is directly imposed) and the ability of well approximating solutions with steep gradient (the scheme introduces exponentials of electric potential differences, which automatically account for the diffusion dominant part and the drift dominant part of the operator). Moreover, the extension to the two-dimensional case is straightforward. The current discretization (in 1-d) can be seen as a non-linear Scharfetter-Gummel discretization [28].

The numerical scheme is applied to the simulation of a one-dimensional n^+nn^+ ballistic diode, which is a simple model of the channel of a MOS transistor. In the numerical simulations, we also use non-parabolic energy bands. The numerical experiments are performed by employing two energy-transport models, the Lyumkis and the Chen model, which are defined by different momentum relaxation time functions. These two models are already used in the physical literature, but only for parabolic band diagrams.

The numerical results show that the energy-transport models describe the velocity overshoot with reasonable accuracy, when compared to the results in the literature (see, e.g., [9]). The spurious velocity overshoot spike at the anode junction becomes smaller in the non-parabolic band case, compared to the parabolic case, and almost vanishes for the Chen model.

2 Formulation of the model

2.1 Scaling of the equations

We bring the equations (1)-(5) into a scaled and dimensionless form. Let C_m be the maximal value of the doping profile, ℓ^* the diameter of the device, μ_0 the low-field mobility constant, T_0 the lattice temperature, and $U_T = k_B T_0/q$ the thermal voltage. Using the scaling

$$\begin{gathered} n \to C_m n, \quad C \to C_m C, \quad T \to T_0 T, \quad V \to U_T V, \quad \mu \to U_T \mu, \quad x \to \ell^* x, \\ J_1 \to (q\mu_0 U_T C_m/\ell^*) J_1, \quad J_2 \to (q\mu_0 U_T^2 C_m/\ell^*) J_2, \\ L_{ij} \to ((qU_T)^{i+j-1}\mu_0 C_m) L_{ij}, \quad W \to (q\mu_0 U_T^2 C_m/\ell^{*2}) W, \end{gathered}$$

we get the system

$$\begin{aligned} -\mathrm{div}\, J_1 &= 0, && (7) \\ -\mathrm{div}\, J_2 &= -J_1 \cdot \nabla V + W, && (8) \\ J_1 &= L_{11}\Big(\nabla \frac{\mu}{T} - \frac{\nabla V}{T}\Big) + L_{12} \nabla\Big(-\frac{1}{T}\Big), && (9) \\ J_2 &= L_{21}\Big(\nabla \frac{\mu}{T} - \frac{\nabla V}{T}\Big) + L_{22} \nabla\Big(-\frac{1}{T}\Big), && (10) \\ \lambda^2 \Delta V &= n - C, && (11) \end{aligned}$$

where $\lambda^2 = \varepsilon_s U_T/(qC_m \ell^{*2})$ denotes the square of the scaled Debye length.

2.2 General non-parabolic band diagrams

In this subsection we reformulate the diffusion coefficients for the energy-transport model (7)-(11), as derived in [5], and we make precise our assumptions on the energy relaxation term. We assume in this and the following subsections that all physical variables and parameters are in scaled form. In order to get more explicit expressions for the coefficients L_{ij} in terms of n, T (or μ, T), we have to impose some physical assumptions:

(H1) The energy-band diagram ε of the semiconductor crystal is spherically symmetric and a strictly monotone function of the modulus $k = |\vec{k}|$ of the wave vector $\vec{k}$. Therefore, the Brillouin zone equals $\mathbb{R}^3$ and $\varepsilon : \mathbb{R} \to \mathbb{R}$, $k \mapsto \varepsilon(k)$.

(H2) A momentum relaxation time can be defined by

$$\tau(\varepsilon) = \Big(\phi_0(2N_0+1)\varepsilon^\beta N(\varepsilon)\Big)^{-1}, \qquad \beta > -2, \quad \phi_0 > 0, \tag{12}$$

where $N(\varepsilon) = 4\pi k^2/|\varepsilon'(k)|$ is the density of states of energy $\varepsilon = \varepsilon(k)$ [5, (III.31)] and N_0 is the phonon occupation number [4, Sec. 4].

(H3) The electron density n and the internal energy E are given by non-degenerate Boltzmann statistics.

The assumptions (H1)–(H2) are imposed in order to get simpler expressions for the variables. In the physical literature, the values $\beta = 0$ [9] and $\beta = 1/2$ [21] have been used in the case of parabolic band structure (see Section 2.4). The non-degeneracy assumption (H3) is valid for semiconductor devices with a doping concentration which is below $10^{19}\mathrm{cm}^{-3}$. Almost all devices in practical applications satisfy this condition.

Under these assumptions, the diffusion coefficients are given by

$$L_{ij} = L_{ij}(\mu, T) = e^{\mu/T}\int_0^\infty d(\varepsilon)\varepsilon^{i+j-2}e^{-\varepsilon/T}d\varepsilon, \tag{13}$$

where

$$d(\varepsilon) = \frac{4\pi}{3}\tau(\varepsilon)|\varepsilon'(k)|k^2 \quad \text{and} \quad \varepsilon = \varepsilon(k)$$

(see [5, (IV.17), (III.33)]). We refer to [5] for more general expressions for the diffusion coefficients under weaker assumptions.

Due to assumption (H3), we have further [5, (IV.16)]

$$n = n(\mu, T) = e^{\mu/T}\int_0^\infty e^{-\varepsilon/T}N(\varepsilon)d\varepsilon, \tag{14}$$

$$E = E(\mu, T) = e^{\mu/T}\int_0^\infty \varepsilon e^{-\varepsilon/T}N(\varepsilon)d\varepsilon. \tag{15}$$

Let $\gamma(\varepsilon) = k^2$ be the inverted $\varepsilon(k)$ relation. Then $N(\varepsilon) = 2\pi\gamma(\varepsilon)^{1/2}\gamma'(\varepsilon)$ and, using (12),

$$d(\varepsilon) = \frac{8\pi}{3}\tau(\varepsilon)\frac{\gamma(\varepsilon)^{3/2}}{\gamma'(\varepsilon)} = \frac{4}{3\phi_0(2N_0+1)}\frac{\gamma(\varepsilon)}{\varepsilon^\beta\gamma'(\varepsilon)^2},$$

which yields

$$L_{ij} = \frac{4}{3\phi_0(2N_0+1)}e^{\mu/T}\int_0^\infty \varepsilon^{i+j-\beta-2}\frac{\gamma(\varepsilon)}{\gamma'(\varepsilon)^2}e^{-\varepsilon/T}d\varepsilon$$

or

$$L_{ij} = T^{i+j-\beta-1} e^{\mu/T} P_\beta(T, i+j) \tag{16}$$

with

$$P_\beta(T,\ell) = \frac{4}{3\phi_0(2N_0+1)} \int_0^\infty u^{\ell-\beta-2} \frac{\gamma(Tu)}{\gamma'(Tu)^2} e^{-u} du.$$

The electron density and the internal energy read (see (14), (15))

$$\begin{aligned} n &= 2\pi e^{\mu/T} \int_0^\infty \gamma(\varepsilon)^{1/2} \gamma'(\varepsilon) e^{-\varepsilon/T} d\varepsilon, \\ E &= 2\pi e^{\mu/T} \int_0^\infty \varepsilon\gamma(\varepsilon)^{1/2} \gamma'(\varepsilon) e^{-\varepsilon/T} d\varepsilon \end{aligned}$$

or

$$n = Te^{\mu/T} Q(T,0), \qquad E = T^2 e^{\mu/T} Q(T,1) \tag{17}$$

with

$$Q(T,\ell) = 2\pi \int_0^\infty u^\ell \gamma(Tu)^{1/2} \gamma'(Tu) e^{-u} du.$$

The energy relaxation term is given by

$$W = \int_0^\infty S_1(e^{(\mu-\varepsilon)/T}) \varepsilon d\varepsilon,$$

where S_1 is the phonon collision operator [5, (IV.18)]. In the Fokker-Planck approximation, we can write this operator as (see [29])

$$S_1(e^{(\mu-\varepsilon)/T}) = \frac{\partial}{\partial\varepsilon} \left\{ \delta(\varepsilon) \left[\left(1 + T_0 \frac{\partial}{\partial\varepsilon}\right) e^{(\mu-\varepsilon)/T} \right] \right\},$$

where $\delta(\varepsilon) = \phi_0 \varepsilon^\beta N(\varepsilon)^2$, $\beta > -1$ and $T_0 = 1$ is the (scaled) ambient temperature. With the definition of $\delta(\varepsilon)$, the above expression can be simplified:

$$\begin{aligned} W &= -e^{\mu/T} \int_0^\infty \delta(\varepsilon) e^{-\varepsilon/T} \left(1 - \frac{T_0}{T}\right) d\varepsilon \\ &= \phi_0 e^{\mu/T} T^\beta (T_0 - T) \int_0^\infty u^\beta N(Tu)^2 e^{-u} du \\ &= 4\pi^2 \phi_0 e^{\mu/T} T^\beta (T_0 - T) \int_0^\infty \gamma(Tu)\gamma'(Tu)^2 u^\beta e^{-u} du. \end{aligned}$$

Introducing

$$R_\beta(T) = \int_0^\infty \gamma(Tu)\gamma'(Tu)^2 u^\beta e^{-u} du, \tag{18}$$

the energy relaxation term can be written as

$$W = \frac{3}{2} \frac{n(T_0 - T)}{\tau_\beta(T)},$$

with the temperature-dependent relaxation time

$$\tau_\beta(T) = \frac{3}{8\pi^2\phi_0} \frac{T^{1-\beta} Q(T,0)}{R_\beta(T)}. \tag{19}$$

2.3 A drift-diffusion formulation for the current densities

A remarkable observation is that the current densities J_1 and J_2 can be written in a drift-diffusion formulation of the type

$$J_1 = \nabla g_1(n,T) - g_1(n,T)\frac{\nabla V}{T}, \tag{20}$$

$$J_2 = \nabla g_2(n,T) - g_2(n,T)\frac{\nabla V}{T}. \tag{21}$$

(Here and in the following, the gradient ∇ always means differentiation with respect to the space variable.) Indeed, in the general case the current densities are given by

$$J_i = \int_0^\infty d(\varepsilon)\left(\nabla e^{(\mu-\varepsilon)/T} + \nabla V \frac{\partial}{\partial\varepsilon} e^{(\mu-\varepsilon)/T}\right)\varepsilon^{i-1} d\varepsilon, \quad i = 1,2. \tag{22}$$

This relation holds true under weak assumptions (see [5] for details) and in particular under the assumptions (H1)–(H3) of Section 2.2.

From (22) we get

$$J_i = \nabla \int_0^\infty d(\varepsilon) e^{(\mu-\varepsilon)/T}\varepsilon^{i-1} d\varepsilon - \frac{\nabla V}{T}\int_0^\infty d(\varepsilon) e^{(\mu-\varepsilon)/T}\varepsilon^{i-1} d\varepsilon$$

which equals (20), (21), respectively, setting

$$g_1 = \int_0^\infty d(\varepsilon) e^{(\mu-\varepsilon)/T} d\varepsilon, \qquad g_2 = \int_0^\infty d(\varepsilon) e^{(\mu-\varepsilon)/T}\varepsilon d\varepsilon.$$

The functions g_1 and g_2 can be computed in terms of n and T, under the assumptions (H1)–(H3) of Section 2.2. Indeed, by (13), we get $g_1 = L_{11}$ and $g_2 = L_{21}$, and using (16) and (17), we can write

$$g_1(n,T) = \frac{P_\beta(T,2)}{Q(T,0)} T^{-\beta} n, \qquad g_2(n,T) = \frac{P_\beta(T,3)}{Q(T,0)} T^{1-\beta} n \tag{23}$$

or

$$g_1(n,T) = \mu_\beta^{(1)}(T) T n, \quad g_2(n,T) = \mu_\beta^{(2)}(T) T^2 n$$

with the temperature-dependent mobilities

$$\mu_\beta^{(i)}(T) = \frac{P_\beta(T,i+1)}{Q(T,0)} T^{-1-\beta}, \quad i = 1,2. \tag{24}$$

We can write the stationary energy-transport model in the drift-diffusion formulation either in the variables n, T and V or in the variables g_1, g_2 and V. In both cases only the current density relations change. In the former case we have

$$J_1 = \nabla(\mu_\beta^{(1)}(T) T n) - \mu_\beta^{(1)}(T) n \nabla V,$$

$$J_2 = \nabla(\mu_\beta^{(2)}(T) T^2 n) - \mu_\beta^{(2)}(T) T n \nabla V,$$

and in the latter case

$$J_i = \nabla g_i - \frac{g_i}{T(g_1,g_2)}\nabla V, \quad i = 1,2.$$

The electron density is given in terms of g_1 and g_2 by, see (23),

$$n(g_1, g_2) = \frac{Q(T(g_1, g_2), 0)}{P_\beta(T(g_1, g_2), 2)} T(g_1, g_2)^\beta g_1. \tag{25}$$

The energy relaxation term in the variables g_1 and g_2 writes now (recall that $T_0 = 1$)

$$W = \frac{3}{2\tau_\beta(T)T} \left(\frac{g_1}{\mu_\beta^{(1)}(T)} - \frac{g_2}{\mu_\beta^{(2)}(T)} \right). \tag{26}$$

In order to compute the electron temperature in terms of g_1 and g_2, we have to invert the following function (see (23)):

$$f(T) \stackrel{\text{def}}{=} \frac{P_\beta(T,3)}{P_\beta(T,2)} T = \frac{g_2}{g_1}. \tag{27}$$

This is possible if and only if the derivative of f is positive for all $T > 0$. The following lemma shows that this is true if and only if the diffusion matrix (L_{ij}) is positive definite. Now, this property has to be satisfied in order to get a well-posed mathematical problem.

Lemma 2.1 *Let the hypotheses (H1)–(H3) hold. Then*

$$f'(T) = \frac{\det(L_{ij})}{(Tg_1)^2}. \tag{28}$$

Proof. Using the relation

$$TP'_\beta(T, \ell - 1) = P_\beta(T, \ell) - (\ell - \beta - 2)P_\beta(T, \ell - 1),$$

which can be proved by integration by parts, we obtain

$$f'(T) = P_\beta(T,2)^{-2}[P_\beta(T,4)P_\beta(T,2) - P_\beta(T,3)^2].$$

Then, from the formulas

$$\det(L_{ij}) = e^{2\mu/T} T^{4-2\beta} [P_\beta(T,4)P_\beta(T,2) - P_\beta(T,3)^2]$$

and $n = Q(T,0)Te^{\mu/T}$ (see (16) and (17)), it follows

$$f'(T) = \Big(\frac{Q(T,0)T^{\beta-1}}{P_\beta(T,2)n} \Big)^2 \det(L_{ij}) = \frac{\det(L_{ij})}{(Tg_1)^2}.$$

For later reference, we rewrite the complete energy-transport model in the (g_1, g_2, V) formulation:

$$\begin{aligned}
-\text{div } J_1 &= 0, && (29)\\
-\text{div } J_2 &= -J_1 \cdot \nabla V + W, && (30)\\
J_1 &= \nabla g_1 - \frac{g_1}{T} \nabla V, && (31)\\
J_2 &= \nabla g_2 - \frac{g_2}{T} \nabla V, && (32)\\
\lambda^2 \Delta V &= n - C(x) \quad \text{in } \Omega, && (33)
\end{aligned}$$

subject to the mixed Dirichlet-Neumann boundary conditions

$$g_1 = g_{D,1}, \quad g_2 = g_{D,2}, \quad V = V_D \qquad \text{on } \Gamma_D, \tag{34}$$
$$J_1 \cdot \nu = J_2 \cdot \nu = \nabla V \cdot \nu = 0 \qquad \text{on } \Gamma_N, \tag{35}$$

where we have set $g_{D,i} = g_i(n_D, T_D)$, $i = 1, 2$. The functions n and W depend on g_1 and g_2 according to (25) and (26), respectively. The dependence of T on g_1 and g_2 is given by the non-linear equation (27).

2.4 A non-parabolic band approximation

In this section we compute the diffusion coefficients and the energy relaxation term for non-parabolic band diagrams in the sense of Kane and we show that for the parabolic band approximation, we get the same relations as in the physical literature [9, 21].

The non-parabolic band structure in the sense of Kane [19] is defined as follows:

(H4) Let the energy $\varepsilon(k)$ satisfy

$$\varepsilon(1 + \alpha\varepsilon) = \frac{k^2}{2m^*}.$$

The constant m^* is the (scaled) effective electron mass given by $m^* = m_0 k_B T_0/\hbar^2 k_0^2$, where m_0 is the unscaled effective mass, k_0 is a typical wave vector, and $\alpha > 0$ is the (scaled) non-parabolicity parameter. Notice that we get a parabolic band diagram if $\alpha = 0$.

The assumption (H4) implies $\gamma(Tu) = 2m^* Tu(1+\alpha Tu)$, and introducing the functions

$$\begin{aligned} p_\beta(\alpha T, \ell) &= \int_0^\infty \frac{1 + \alpha Tu}{(1 + 2\alpha Tu)^2} u^{\ell-\beta-1} e^{-u} du, \\ q(\alpha T, \ell) &= \int_0^\infty (1 + \alpha Tu)^{1/2}(1 + 2\alpha Tu) u^{1/2+\ell} e^{-u} du, \end{aligned}$$

we can rewrite P_β and Q as (see Section 2.2)

$$\begin{aligned} P_\beta(T, \ell) &= \frac{2}{3\phi_0(2N_0 + 1)m^*} T p_\beta(\alpha T, \ell), \\ Q(T, \ell) &= 2\pi(2m^*)^{3/2} T^{1/2} q(\alpha T, \ell). \end{aligned}$$

Therefore, the electron density and internal energy from (17) become

$$n = N(T) T^{3/2} e^{\mu/T}, \quad E = \frac{q(\alpha T, 1)}{q(\alpha T, 0)} Tn,$$

where $N(T) = 2\pi(2m^*)^{3/2} q(\alpha T, 0)$. For the mobilities (24) we get the expressions

$$\mu_\beta^{(i)}(T) = \mu_0 \frac{p_\beta(\alpha T, i+1)}{q(\alpha T, 0)} T^{-1/2-\beta}, \quad i = 1, 2.$$

Here, the mobility constant μ_0 is given by

$$\mu_0 = \left(3\pi\phi_0(2N_0 + 1)m^*(2m^*)^{3/2}\right)^{-1}.$$

Furthermore, introducing

$$r_\beta(\alpha T) = \int_0^\infty (1+\alpha T u)(1+2\alpha T u)^2 u^{1+\beta} e^{-u} du,$$

we obtain (see (18))

$$R_\beta(T) = (2m^*)^3 r_\beta(T) T,$$

and the energy relaxation time (19) becomes

$$\tau_\beta(T) = \tau_0 \frac{3q(\alpha T, 0)}{2 r_\beta(\alpha T)} T^{1/2-\beta},$$

where

$$\tau_0 = \Big(2\pi\phi_0 (2m^*)^{3/2}\Big)^{-1}.$$

Notice that the function r_β is in fact a polynomial:

$$r_\beta(\alpha T) = \Gamma(\beta+2) + 5\Gamma(\beta+3)\alpha T + 8\Gamma(\beta+4)(\alpha T)^2 + 4\Gamma(\beta+5)(\alpha T)^3.$$

The symbol Γ denotes the Gamma function defined by

$$\Gamma(s) = \int_0^\infty u^{s-1} e^{-u} du, \quad s > 0.$$

(Here we use the hypothesis $\beta > -2$.)

Finally, the energy relaxation term (26) can be rewritten as

$$W = \frac{T^{2\beta-1}}{\mu_0 \tau_0} r_\beta(\alpha T) \left(\frac{g_1}{p_\beta(\alpha T, 2)} - \frac{g_2}{p_\beta(\alpha T, 3)} \right).$$

In the parabolic band approximation case ($\alpha = 0$) the above expressions simplify. Since $q(0,0) = \Gamma(3/2) = \sqrt{\pi}/2$ and $q(0,1) = \Gamma(5/2) = 3\sqrt{\pi}/4$, we get for the electron density and the internal energy the well-known relations

$$n = (2\pi m^*)^{3/2} T^{3/2} e^{\mu/T}, \quad E = \frac{3}{2} T n.$$

In order to compute the mobilities and the energy relaxation time, we have to specify the parameter β. As mentioned in Section 2.2, in the literature the values $\beta = 1/2$ (used by Chen *et al.*, cf. [9]) and $\beta = 0$ (used by Lyumkis *et al.*, cf. [21]) have been employed.

First let $\beta = 1/2$. Then $p_{1/2}(0,2) = \sqrt{\pi}/2$ and $p_{1/2}(0,3) = r_{1/2}(0) = 3\sqrt{\pi}/4$ and therefore,

$$\mu_{1/2}^{(1)}(T) = \mu_0 T^{-1}, \quad \mu_{1/2}^{(2)}(T) = \frac{3}{2}\mu_0 T^{-1}, \quad \tau_{1/2}(T) = \tau_0.$$

Hence, we get the same current density relations and the same energy relaxation term as Chen *et al.* in [9]:

$$\begin{aligned} J_1 &= \mu_0 \Big(\nabla n - \frac{n}{T} \nabla V \Big), \\ J_2 &= \frac{3}{2}\mu_0 \Big(\nabla(nT) - n\nabla V \Big), \\ W &= \frac{3}{2} \frac{n(T_0 - T)}{\tau_0}. \end{aligned}$$

The energy-transport model with the above relations will be called the *Chen model.*

When $\beta = 0$, we have $p_0(0,2) = r_0(0) = 1$, $p_0(0,3) = 2$ and

$$\mu_0^{(1)}(T) = \frac{2\mu_0}{\sqrt{\pi}} T^{-1/2}, \quad \mu_0^{(2)}(T) = \frac{4\mu_0}{\sqrt{\pi}} T^{-1/2}, \quad \tau_0(T) = \frac{3\sqrt{\pi}}{4}\tau_0 T^{1/2},$$

so that the current densities and the energy relaxation term become

$$\begin{aligned} J_1 &= \frac{2\mu_0}{\sqrt{\pi}}\Big(\nabla(nT^{1/2}) - \frac{n}{T^{1/2}}\nabla V\Big), \\ J_2 &= \frac{4\mu_0}{\sqrt{\pi}}\Big(\nabla(nT^{3/2}) - nT^{1/2}\nabla V\Big), \\ W &= \frac{2}{\sqrt{\pi}}\frac{n(T_0 - T)}{\tau_0 T^{1/2}}. \end{aligned}$$

The energy transport equations with these expressions will be called the *Lyumkis model.*

We conclude this section with a remark on the choice of the parameters. In order to determine the energy-transport model completely, the parameters α, β, ϕ_0, N_0 and k_0 have to be chosen. The mobility constant μ_0 depends on ϕ_0, N_0 and k_0 (the dependence on k_0 comes in via m^*), and the constant τ_0 depends on ϕ_0 and k_0. Instead of choosing the parameters ϕ_0, N_0 and k_0, we prescribe μ_0 and τ_0 whose values (depending on the semiconductor material) can be derived from physical experiments.

3 Numerical approximation

In the following we describe in detail the discretization of the one-dimensional energy flux continuity equations (30), (32) by means of an exponential fitting mixed finite element method. The discretization of equations (29), (31) is similar but simpler (since the zero-th order term and the right-hand side of (29) are zero). The Poisson equation (33) is discretized with a P_1 finite element scheme. Consequently, in the following V denotes a piecewise linear function and V_x its (piecewise constant) derivative. The exponential fitting mixed finite element method introduced for the drift-diffusion continuity equation (cf. [6, 7, 8, 23]) can be sketched as follows: *(i)* transformation of the problem by means of the Slotboom variable to a symmetric form; *(ii)* discretization of the symmetric form with mixed finite elements (consequently, the flux is introduced as independent variable); *(iii)* suitable discrete change of variable to rewrite the equations in terms of the original variables g_2. Due to the non-constant electron temperature, a Slotboom variable does not exist in the present case. As starting point of the discretization scheme we define a "local" Slotboom variable, assuming that the temperature is a prescribed piecewise constant function defined in the global iteration process. We refer to the end of the section for an explicit choice of the procedure. A related idea has been used in [18] for the discretization of the non-linear drift-diffusion continuity equation.

More precisely, introduce a partition $0 = x_0 < x_1 < \cdots < x_N = 1$ of $(0,1)$ and set $I_i = (x_{i-1}, x_i)$, $h_i = x_i - x_{i-1}$ for $i = 1, \ldots, N$, and $h = \max_i h_i$. We denote by $\overline{T}$ the piecewise constant approximation of the temperature (see (57) for the precise definition). The equations to be solved are then

$$\begin{aligned} J_2 &= (g_2)_x - g_2 V_x/\overline{T}, && (36) \\ -(J_2)_x + \overline{c}_2 g_2 &= -J_1 V_x + \overline{c}_1 g_1, && (37) \end{aligned}$$

where we set

$$\overline{c}_\ell = \frac{3}{2\overline{T}\tau_\beta(\overline{T})\mu_\beta^{(\ell)}(\overline{T})},$$

for $\ell = 1, 2$, and, for simplicity of notation, we denote again by J_ℓ, g_ℓ, for $\ell = 1, 2$ the variables.

In each interval I_i, "local" Slotboom variables are introduced by

$$y_2 = e^{-V/\overline{T}} g_2 \quad \text{in } I_i, \tag{38}$$

and equations (36) and (37) are written in the interval I_i as:

$$e^{-V/\overline{T}} J_2 - (y_2)_x = 0, \tag{39}$$

$$-(J_2)_x + \overline{c}_2 e^{V/\overline{T}} y_2 = -J_1 V_x + \overline{c}_1 g_1. \tag{40}$$

A similar idea for the transformation of the energy-transport equations has been used in [16]. Jerome and Shu [14, 15] have employed a slightly different Slotboom transformation by introducing $\phi(x) = \int_0^x V_x(s)/T(s)ds$.

To define the mixed finite element scheme we follow [23], where a monotonic scheme for the 2-dimensional current continuity equation in the presence of zero-th order term has been developed. The finite dimensional space for the flux variable contains functions of $L^2(\Omega)$, which are in each interval polynomials of the form $\sigma(x) = a_i + b_i P_i(x)$, with a_i, b_i constant and $P_i(x)$ a second order polynomial uniquely defined in the interval I_i as follows. Let $P(x)$ be the second order polynomial with the following properties:

$$\int_0^1 P(x)dx = 0, \quad P(0) = 0, \quad P(1) = 1, \tag{41}$$

that is, $P(x) = 3x^2 - 4x + 1$. Moreover, it holds $\int_0^1 P'(x)dx = 1, \int_0^1 P(x)^2 dx = \frac{2}{15}$. We define $P_i(x)$ (depending on V) by

$$P_i(x) \quad = -P(\tfrac{x_i - x}{h_i}) \qquad \text{if } i_{min} = i - 1, \tag{42}$$

$$P_i(x) \quad = P(\tfrac{x - x_{i-1}}{h_i}) \qquad \text{if } i_{min} = i, \tag{43}$$

where i_{min} is the point of minimum of the potential $V(x)$ in the interval I_i. We shall denote by V_{min} its minimum value. Notice that the minimum is always attained at one end point of the interval, since V is linear in I_i. If $V(x)$ is constant in I_i, we define $P_i(x) = P(\frac{x - x_{i-1}}{h_i})$.

Let us introduce the following finite dimensional spaces:

$$\begin{aligned}
X_h &= \{\sigma \in L^2(\Omega) \,:\, \sigma(x) = a_i + b_i P_i(x) \text{ in } I_i,\ i = 1, \ldots, N\}, \\
W_h &= \{\xi \in L^2(\Omega) \,:\, \xi \text{ is constant in } I_i,\ i = 1, \ldots, N\}, \\
\Lambda_{h,\chi} &= \{q \text{ is defined at the nodes } x_0, \ldots, x_N\, q(x_0) = \chi(0),\ q(x_N) = \chi(1)\}.
\end{aligned}$$

The mixed–hybrid approximation of equations (36)-(37) is then:

Find $J_2^h \in X_h$, $\overline{g}_2^h \in W_h$, $g_2^h \in \Lambda_{h,g_{D,2}}$, such that :

$$\sum_{i=1}^N \left(\int_{I_i} A_i J_2^h \sigma + \int_{I_i} B_i \overline{g}_2^h \sigma_x - \left[e^{-V/\overline{T}} g_2^h \sigma \right]_{x_{i-1}}^{x_i} \right) = 0, \tag{44}$$

$$\sum_{i=1}^{N}\left(-\int_{I_i}(J_2^h)_x\xi+\int_{I_i}\overline{c}_2\overline{g}_2^h\xi\right)=\sum_{i=1}^{N}\int_{I_i}(-J_1^hV_x+\overline{c}_1\overline{g}_1^h)\xi, \tag{45}$$

$$\sum_{i=1}^{N}[qJ_2^h]_{x_{i-1}}^{x_i}=0, \tag{46}$$

for all $\sigma\in X_h$, $\xi\in W_h$, $q\in\Lambda_{h,0}$. $J_1^h\in X_h$ is the approximation of the current density J_1, $\overline{g}_1^h\in W_h$ is the piecewise constant approximation of g_1, stemming from the discretization of the current continuity equation (see (54)-(56) below). In the first equation A and B denote the piecewise constant functions (approximation of $e^{-V/\overline{T}}$) defined in each interval I_i by

$$\begin{aligned} A|_{I_i} &= A_i \stackrel{\text{def}}{=} \frac{1}{h_i}\int_{x_{i-1}}^{x_i} e^{-V(s)/\overline{T}}ds, \quad i=1,\dots,N,\\ B|_{I_i} &= B_i \stackrel{\text{def}}{=} e^{-V_{min}/\overline{T}}, \quad\quad i=1,\dots,N. \end{aligned}$$

J_2^h is an approximation of the energy flux J_2, $\overline{g}_2^h$ is a piecewise constant approximation of g_2 and g_2^h is an approximation of g_2 at the nodes (see [3, 22]). The first equation is obtained from a weak version of (39), using integration by parts and summation over all I_i together with the inverse of the Slotboom transformation (38). Notice that the discrete inverse transformation is not the same for the variables $\overline{g}_2^h$ and g_2^h. We refer to [23] for a detailed discussion on the need of different approximations of the exponential function due to (possibly) large value of V_x. The second equation is a discrete weak version of (37), obtained from (40) where $e^{V/\overline{T}}$ is approximated by B^{-1} and the discrete inverse Slotboom transformation for $\overline{g}_2^h$ is used. The third equation implies the continuity of J_2^h at the nodes.

The variables J_2^h and $\overline{g}_2^h$ can be eliminated a priori by static condensation, leading to a final algebraic system in the variables g_2^h only. We write $J_2^h\in X_h$ as

$$J_2^h(x)=J_{2,i}^0+J_{2,i}^1P_i(x)\quad\text{for } x\in I_i, \tag{47}$$

for some constants $J_{2,i}^0$, $J_{2,i}^1$, $i=1,\dots,N$. Set $\overline{g}_{2,i}=\overline{g}_2^h|_{I_i}$, $g_{2,i}=g_2^h(x_i)$, $V_i=V(x_i)$ and $q_i=q(x_i)$. Taking $\sigma\in X_h$ such that $\sigma=1$ in I_i and $\sigma=0$ elsewhere in equation (44) gives

$$h_iA_iJ_{2,i}^0=e^{-V_i/\overline{T}}g_{2,i}-e^{-V_{i-1}/\overline{T}}g_{2,i-1}.$$

The integral in the definition of A_i can be computed explicitly and we arrive after elementary computations to

$$J_{2,i}^0=\frac{V_i-V_{i-1}}{2\overline{T}}\coth\Big(\frac{V_i-V_{i-1}}{2\overline{T}}\Big)\frac{g_{2,i}-g_{2,i-1}}{h_i}-\frac{g_{2,i}+g_{2,i-1}}{2\overline{T}}\frac{V_i-V_{i-1}}{h_i}. \tag{48}$$

This discretization can be seen as a non-linear Scharfetter-Gummel scheme (cf. [6]). The constants $J_{2,i}^1$ are computed by using (45) once $\overline{g}_{2,i}$ is given. Indeed, taking $\xi=1$ in I_i and $\xi=0$ elsewhere in equation (45), it follows

$$J_{2,i}^1=\overline{c}_2h_i\overline{g}_{2,i}-h_ir_i, \tag{49}$$

where we set $r_i = \frac{1}{h_i}\int_{I_i}(-J_1^h V_x + \overline{c}_1 \overline{g}_1^h)dx$. Taking now $\sigma \in X_h$ such that $\sigma = P_i(x)$ in I_i and $\sigma = 0$ elsewhere in equation (44) we obtain

$$\frac{2}{15} h_i A_i J_{2,i}^1 = -e^{-V_{min}/\overline{T}} \overline{g}_{2,i} + e^{-V_{min}/\overline{T}} g_{2,i_{min}}. \tag{50}$$

Using (49) and (50), we can eliminate $J_{2,i}^1$ and get

$$\overline{g}_{2,i}^h = (\overline{\gamma}\ \overline{c}_2 + 1)^{-1}(\overline{\gamma} r_i + g_{2,i_{min}}), \tag{51}$$

where $\overline{\gamma} = \frac{2}{15} h_i^2 A_i e^{V_{min}}$. Replacing (51) into (49) we get $J_{2,i}^1$ in terms of $g_{2,i}$:

$$J_{2,i}^1 = \frac{\overline{c}_2 h_i}{\overline{\gamma}\ \overline{c}_2 + 1} g_{2,i_{min}} - \frac{h_i}{\overline{\gamma}\ \overline{c}_2 + 1} r_i. \tag{52}$$

Finally, equation (46), with $q_i = 1$ and $q_k = 0$ for all $k \neq i$, gives

$$J_{2,i}^0 + J_{2,i}^1 P_i(x_i) = J_{2,i+1}^0 + J_{2,i+1}^1 P_{i+1}(x_i), \qquad i = 1, \ldots, N. \tag{53}$$

We recall that, due to definition (41)-(43), $P_i(x_i) = 0$ ($P_{i+1}(x_i) = 0$, resp.) if the minimum of V on I_i is in x_{i-1} (x_{i+1}, resp.), otherwise it is $P_i(x_i) = 1$ ($P_{i+1}(x_i) = -1$, resp.). Using the expression (48) for $J_{2,i}^0$ and (52) for $J_{2,i}^1$, the last equation (53) can be written in terms of the variables $g_{2,i}$ only, giving rise to a tridiagonal algebraic system, with the (positive) contribution of the zero-th order term appearing only in the diagonal entry. Then the energy flux J_2^h is computed locally in each interval by (47) and $\overline{g}_2^h$ is computed locally by (51).

Discretizing the current continuity equation (29), (31) with the same scheme and applying the (simpler) static condensation procedure (J_1^h is piecewise constant in this case), we obtain

$$J_{1,i}^0 = J_{1,i+1}^0 \qquad i = 1, \ldots, N, \tag{54}$$

with

$$J_{1,i}^0 = \frac{V_i - V_{i-1}}{2\overline{T}} \coth\Big(\frac{V_i - V_{i-1}}{2\overline{T}}\Big)\frac{g_{1,i} - g_{1,i-1}}{h_i} - \frac{g_{1,i} + g_{1,i-1}}{2\overline{T}}\frac{V_i - V_{i-1}}{h_i}. \tag{55}$$

Moreover, the analogous of (51) gives the upwind expression

$$\overline{g}_{1,i} = g_{1,i_{min}}, \qquad i = 1, \ldots, N. \tag{56}$$

In order to complete the scheme, we still have to specify how the piecewise constant temperature $\overline{T}$ is defined. The temperature is defined implicitly in terms of g_1 and g_2 according to the non-linear equation (27). Lemma 2.1 shows that this equation can be solved uniquely. Numerically, we define $\overline{T}$ in each interval I_i as approximate solution of

$$\frac{\overline{g}_{2,i}}{\overline{g}_{1,i}} = f(\overline{T}_i), \qquad i = 1, \ldots, N, \tag{57}$$

with $\overline{T}_i \stackrel{\text{def}}{=} \overline{T}|_{I_i}$ and $\overline{g}_{1,i}$, $\overline{g}_{2,i}$ given by the mixed scheme (see (56), (51)). The non-linear equation reduces to a linear one when $\alpha = 0$ (parabolic band). For $\alpha > 0$ a single iteration of the (scalar) Newton scheme is sufficient to obtain $\overline{T}$ with an accuracy of 10^{-8}, when the initial guess is the temperature at the previous global iteration procedure step. Moreover, f' can be explicitly computed by (28).

In contrast to the strongly coupled equations (7)-(10) in the variables μ/T and $-1/T$, the two continuity equations (29) and (30) are *weakly* coupled through the temperature (which varies only slowly during the iterations). Consequently, we defined the global iteration procedure as follows. The temperature is frozen at the previous iteration step, and a full Newton method is used to solve the non-linear system in g_1, g_2 and V. At each iteration, the temperature is updated according to equation (57). The associated linear system is solved by using a GMRES solver. Finally, we remark that a Gummel-type iteration procedure can be employed (instead of the Newton method) in the parabolic band case.

4 Numerical results

As a numerical example we present the simulation of a one-dimensional n^+nn^+ ballistic silicon diode which is a simple model for the channel of a MOS transistor. The semiconductor domain is given by the interval $\Omega = (0, \ell^*)$ with $\ell^* > 0$. In the n^+-regions the maximal doping concentration is $5 \cdot 10^{17}\,\mathrm{cm}^{-3}$; in the n-channel the minimal doping profile is $2 \cdot 10^{15}\,\mathrm{cm}^{-3}$. The doping profile is shown in Figure 1. The length of the n^+-regions is $0.1\,\mu$m, whereas the length of the channel region equals $0.4\,\mu$m. The numerical values of

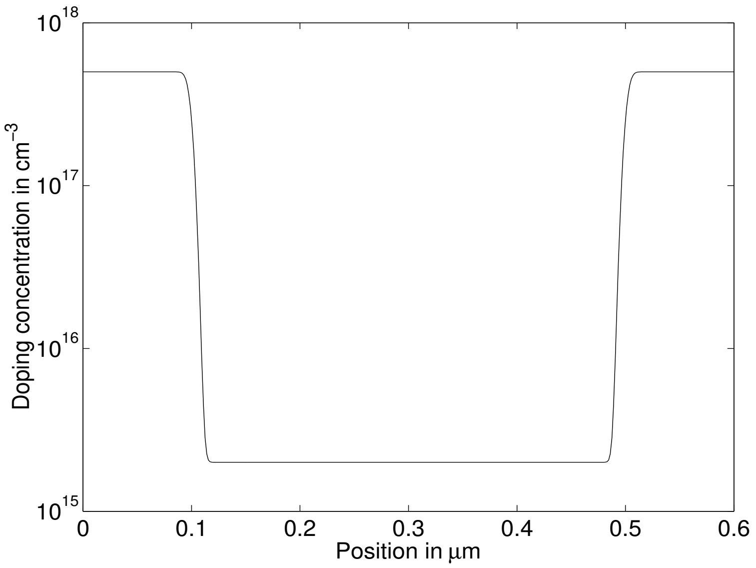

Figure 1: Doping concentration in the n^+nn^+ diode.

the physical parameters (for a silicon diode) are given in Table 1.

On the boundary points $x = 0$ and $x = \ell^*$ we assume that the (unscaled) total space charge $C - n$ vanishes and that the (unscaled) temperature has the ambient temperature:

$$n(0) = n(\ell^*) = c_1, \qquad T(0) = T(\ell^*) = T_0, \qquad V(0) = 0, \quad V(\ell^*) = U,$$

where $U > 0$ is the applied voltage. We take the value $U = 1.5\,\mathrm{V}$. The unscaled relaxation time τ_0 and the low-field mobility μ_0 depend on ϕ_0 and k_0 (see Section 2.4). These parameters are chosen such that τ_0 and μ_0 take the values shown in Table 1. We have

Parameter	Physical meaning	Numerical value
q	elementary charge	$1.6 \cdot 10^{-19}\,\mathrm{As}$
ε_s	permittivity constant	$10^{-12}\,\mathrm{AsV^{-1}cm^{-1}}$
μ_0	(low field) mobility constant	$1.5 \cdot 10^3\,\mathrm{cm^2V^{-1}s^{-1}}$
U_T	thermal voltage at $T_0 = 300\,\mathrm{K}$	$0.026\,\mathrm{V}$
ℓ^*	length of the device	$0.6\,\mu\mathrm{m}$
ℓ_0	length of the n^+ region	$0.1\,\mu\mathrm{m}$
c_0	doping concentration in the n region	$2 \cdot 10^{15}\,\mathrm{cm^{-3}}$
c_1	doping concentration in the n^+ region	$5 \cdot 10^{17}\,\mathrm{cm^{-3}}$
τ_0	energy relaxation time	$0.4 \cdot 10^{-12}\,\mathrm{s}$
α	non-parabolicity parameter	$0.5\,(\mathrm{eV})^{-1}$

Table 1: Physical parameters.

chosen the data such that our results can be compared to the numerical results of the literature (see, e.g., [9, 26, 31]).

We perform numerical results for a uniform mesh of 100 nodes. In Figure 2 we present the electron temperature for vanishing and non-vanishing non-parabolicity parameter α using Lyumkis' model. As expected the temperature in the n-channel is high, i.e. the electrons are 'hot'. The maximal temperature for $\alpha = 0$ is $T = 3970\,\mathrm{K}$ and $T = 3240\,\mathrm{K}$ for $\alpha = 0.5\,(\mathrm{eV})^{-1}$. The corresponding thermal energies are $E_{th} = \frac{3}{2}k_B T = 0.51\,\mathrm{eV}$ and $E_{th} = 0.42\,\mathrm{eV}$, respectively. Therefore, the temperature is reduced due to the non-parabolicity effects. Similar results can be observed by employing Chen's model (Figure 3). Here, the maximal temperature (thermal energy) values are $T = 2330\,\mathrm{K}$ ($E_{th} = 0.30\,\mathrm{eV}$) for $\alpha = 0$ and $T = 1610\,\mathrm{K}$ ($E_{th} = 0.21\,\mathrm{eV}$) for $\alpha = 0.5\,(\mathrm{eV})^{-1}$. The *effective* scaled relaxation time in the Lyumkis model is $(3\sqrt{\pi}/4)\tau_0\sqrt{T}$ and τ_0 in the Chen model. Therefore, the effective relaxation time in the Chen model is smaller than that in the Lyumkis model, and we expect that the maximal temperature in the Chen model is smaller than in the Lyumkis model. This observation follows from the fact that in the vanishing relaxation-time limit, the temperature relaxes to the lattice temperature, and it is confirmed by our numerical experiments.

In Figure 4 the electron mean velocity for the two different values of the non-parabolicity parameter α using Lyumkis' model is shown. The mean velocity u is defined by $u = J_1/(qn)$. The spurious velocity overshoot peak at the left junction becomes smaller for non-vanishing non-parabolicity parameter. The maximal mean velocity for $\alpha = 0$ is $u = 2.92 \cdot 10^7\,\mathrm{cm/s}$ and $u = 1.51 \cdot 10^7\,\mathrm{cm/s}$ for $\alpha = 0.5\,(\mathrm{eV})^{-1}$. The same effect can be observed using Chen's model (see Figure 5), where the spurious velocity overshoot spike almost vanishes for $\alpha = 0.5\,(\mathrm{eV})^{-1}$. The maximal velocities are $u = 1.44 \cdot 10^7\,\mathrm{cm/s}$ for $\alpha = 0$ and $u = 1.25 \cdot 10^7\,\mathrm{cm/s}$ for $\alpha = 0.5\,(\mathrm{eV})^{-1}$.

The mean velocities for the non-parabolic case, using Chen's or Lyumkis' models, are compared to the mean velocity from the standard drift-diffusion model in Figure 6. In the latter model, no velocity saturation effects are taken into account, i.e. the drift-diffusion model equals the energy-transport equations in the case of *constant* temperature. The velocity overshoot from the drift-diffusion model is much larger than for the energy-transport equations (Figure 6). This can be explained by the fact that the total energy

Model	slope
Lyumkis: $\alpha = 0.0$	1.00
Lyumkis: $\alpha = 0.5/\text{eV}$	0.88
Chen: $\alpha = 0.0$	0.90
Chen: $\alpha = 0.5/\text{eV}$	0.90

Table 2: Slopes of the logarithmic current-voltage curves for $U \in [0.5\text{V}, 1.5\text{V}]$.

of the energy-transport model is composed of the thermal *and* the kinetic energy, whereas the total energy of the drift-diffusion model is determined only by the kinetic energy.

In Figure 7 we present the current-voltage characteristics for the different energy-transport models. The particle current density J_1 is always smaller in non-parabolic band situations. Its dependence on the applied voltage U seems to be sublinear. Indeed, in the voltage range $U \in [0.5\text{V}, 1.5\text{V}]$, the dependence of J_1 on U is approximately $J_1 \sim U^\gamma$, where γ is between 0.88 and 1. depending on the model (see Table 2). We remark that increasing the number of nodes does not change the values of the current.

5 Conclusions

In this paper we have derived energy-transport models for semiconductors for general non-parabolic band diagrams. The diffusion coefficients and the energy relaxation term can be written analytically in terms of the electron density and the temperature if non-parabolic bands in the sense of Kane are considered. The energy-transport models are completely derived from the semiconductor Boltzmann equation. There appear two parameters: the non-parabolicity parameter α and the parameter in the definition of the momentum relaxation time β. For parabolic bands ($\alpha = 0$), we recover two models already studied in the literature: the so-called Lyumkis model ($\beta = 0$) [21] and the so-called Chen model ($\beta = 1/2$) [9].

Thanks to a drift-diffusion formulation valid for a large class of energy-transport models, we presented a mixed exponential fitting finite element discretization of the stationary equations and numerical experiments of a ballistic diode in one space dimension. It turns out that the spurious velocity overshoot peak is smaller in Chen's model than in Lyumkis' model and for non-parabolic bands compared to parabolic ones. Furthermore, the spurious peak almost vanishes in the non-parabolic Chen model. This shows that the energy-transport models describe the charge flow of electrons in a ballistic diode with reasonable accuracy.

References

[1] W. Allegretto and H. Xie. Nonisothermal semiconductor systems. In X. Liu and D. Siegel, editors, *Comparison methods and stability theory*, volume 162 of *Lecture Notes in Pure and Applied Mathematics*, New York, 1994. Marcel Dekker.

[2] Y. Apanovich, P. Blakey, R. Cottle, E. Lyumkis, B. Polsky, A. Shur, and A. Tcherniaev. Numerical simulations of submicrometer devices including coupled nonlocal transport and nonisothermal effects. *IEEE Trans. El. Dev.*, 42:890–897, 1995.

[3] D. N. Arnold and F. Brezzi. Mixed and nonconforming finite element methods: Implementation, postprocessing and error estimates. *RAIRO, Mod. Math. Anal. Numer.* 19:7–32, 1985.

[4] N. Ben Abdallah, P. Degond, P. Markowich and C. Schmeiser. High field approximations of the spherical harmonics expansion model for semiconductors. Submitted for publication, 1999.

[5] N. Ben Abdallah and P. Degond. On a hierarchy of macroscopic models for semiconductors. *J. Math. Phys.*, 37:3308–3333, 1996.

[6] F. Brezzi, L. Marini, and P. Pietra. Méthodes d'éléments finis mixtes et schéma de Scharfetter-Gummel. *C. R. Acad. Sci. Paris*, 305:599–604, 1987.

[7] F. Brezzi, L. Marini, and P. Pietra. Numerical simulation of semiconductor devices. *Comp. Meth. Appl. Mech. Engrg.*, 75:493–514, 1989.

[8] F. Brezzi, L. Marini, and P. Pietra. Two-dimensional exponential fitting and applications to drift-diffusion models. *SIAM J. Num. Anal.*, 26:1342–1355, 1989.

[9] D. Chen, E. Kan, U. Ravaioli, C. Shu, and R. Dutton. An improved energy transport model including nonparabolicity and non-maxwellian distribution effects. *IEEE Electr. Dev. Letters*, 13:26–28, 1992.

[10] D. Chen, E. Sangiorgi, M. Pinto, E. Kan, U. Ravaioli, and R. Dutton. Analysis of spurious velocity overshoot in hydrodynamic simulations. *NUPAD IV*, pages 109–114, 1992.

[11] P. Degond, S. Génieys, and A. Jüngel. An existence and uniqueness result for the stationary energy-transport model in semiconductor theory. *C. R. Acad. Sci. Paris*, 324:29–34, 1997.

[12] P. Degond, S. Génieys, and A. Jüngel. A system of parabolic equations in nonequilibrium thermodynamics including thermal and electrical effects. *J. Math. Pures Appl.*, 76:991–1015, 1997.

[13] P. Degond, S. Génieys, and A. Jüngel. A steady-state system in nonequilibrium thermodynamics including thermal and electrical effects. *Math. Meth. Appl. Sci.*, 21:1399-1413, 1998.

[14] J. Jerome. *Analysis of charge transport. A mathematical study of semiconductor devices.* Springer, Berlin, 1996.

[15] J. Jerome and C.-W. Shu. Energy transport systems for semiconductors: Analysis and simulation. In *Proccedings of the First World Congress of Nonlinear Analysts*, Berlin, 1995. Walter de Gruyter.

[16] A. Jüngel. The energy-transport model for semiconductors: some analytical and numerical results. In *Proceedings of the International Workshop on "Recent Progress in the Mathematical Theory on Vlasov-Maxwell Equations" in Paris*, pages 140–158, 1997.

[17] A. Jüngel. Regularity and uniqueness of solutions to a system of parabolic equations in nonequilibrium thermodynamics. To appear in *Nonlin. Anal. TMA*, 1999.

[18] A. Jüngel and P. Pietra. A discretization scheme of a quasi-hydrodynamic semiconductor model. *Math. Models Meth. Appl. Sci.*, 7:935–955, 1997.

[19] E. Kane. *J. Phys. Chem. Solids*, 1:249, 1957.

[20] T. Kerkhoven and Y. Saad. On acceleration methods for coupled nonlinear elliptic systems. *Num. Math.*, 60:525–548, 1992.

[21] E. Lyumkis, B. Polsky, A. Shur, and P. Visocky. Transient semiconductor device simulation including energy balance equation. *Compel*, 11:311–325, 1992.

[22] L.D. Marini and P. Pietra. An abstract theory for mixed approximations of second order elliptic problems. *Mat. Aplic. Comp.*, 8:219–239, 1989.

[23] L.D. Marini and P. Pietra. New mixed finite element schemes for current continuity equations. *COMPEL*, 9:257–268, 1990.

[24] P. A. Markowich. *The Stationary Semiconductor Device Equations.* Springer, Wien, 1986.

[25] P. A. Markowich, C. A. Ringhofer, and C. Schmeiser. *Semiconductor Equations.* Springer, 1990.

[26] A. Marrocco, P. Montarnal, and B. Perthame. Simulation of the energy-transport and simplified hydrodynamic models for semiconductor devices using mixed finite elements. In *Proceedings ECCOMAS 96*, London, 1996. John Wiley.

[27] P. Raviart and J. Thomas. A mixed finite element method for second order elliptic equations. In *Mathematical Aspects of the Finite Element Method*, volume 606 of *Lecture Notes in Math.*, pages 292–315. Springer, 1977.

[28] D. Scharfetter and H. Gummel. Large signal analysis of a Silicon Read diode oscillator. *IEEE Trans. El. Dev.*, ED–16:64–77, 1969.

[29] C. Schmeiser and A. Zwirchmayr. Elastic and drift-diffusion limits of electron-phonon interaction in semiconductors. *Math. Mod. Meth. Appl. Sci.*, 8:37-53, 1998.

[30] K. Souissi, F. Odeh, and A. Gnudi. A note on current discretization in the hydromodel. *Compel*, 10:475–485, 1991.

[31] K. Souissi, F. Odeh, H. Tang, and A. Gnudi. Comparative studies of hydrodynamic and energy transport models. *Compel*, 13:439–453, 1994.

[32] P. Visocky. A method for transient semiconductor device simulation using hot-electron transport equations. In J. Miller, editor, *Proc. of the Nasecode X Conf.*, Dublin, 1994. Boole Press.

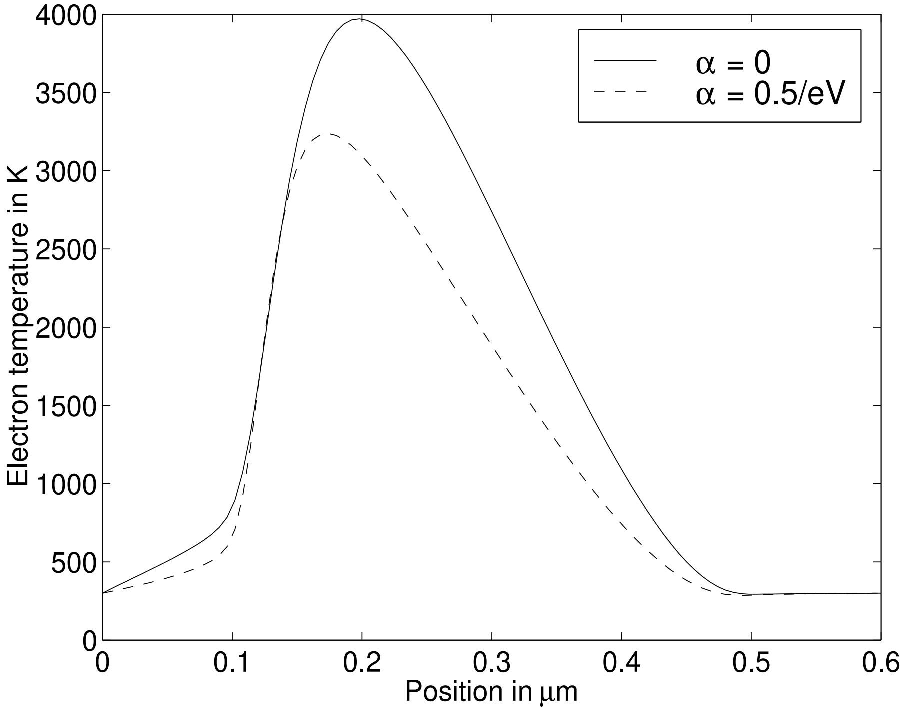

Figure 2: Electron temperature versus position in a ballistic diode using Lyumkis' model.

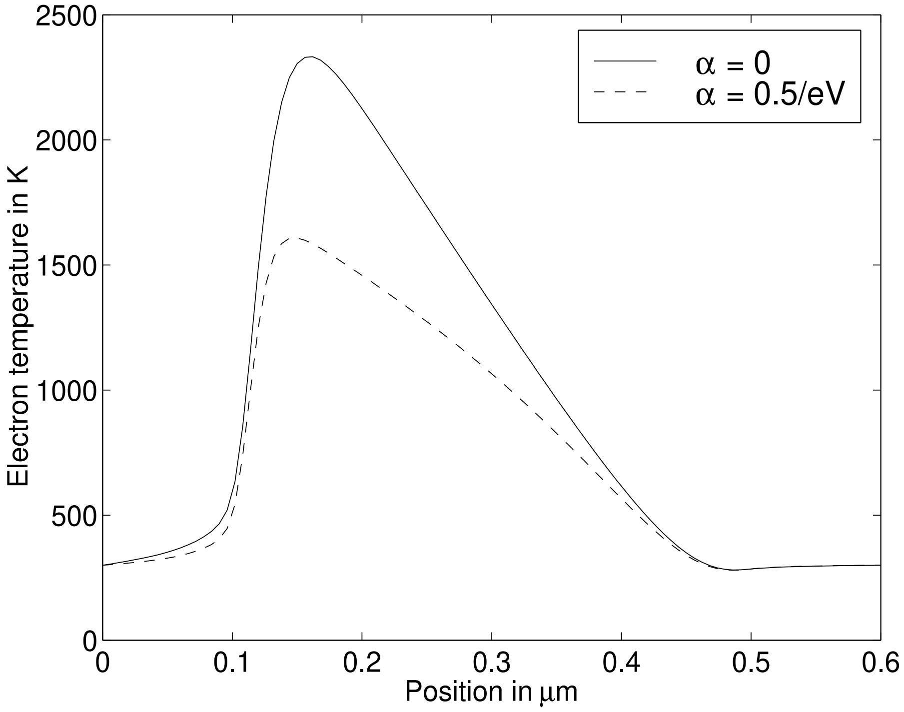

Figure 3: Electron temperature versus position in a ballistic diode using Chen's model.

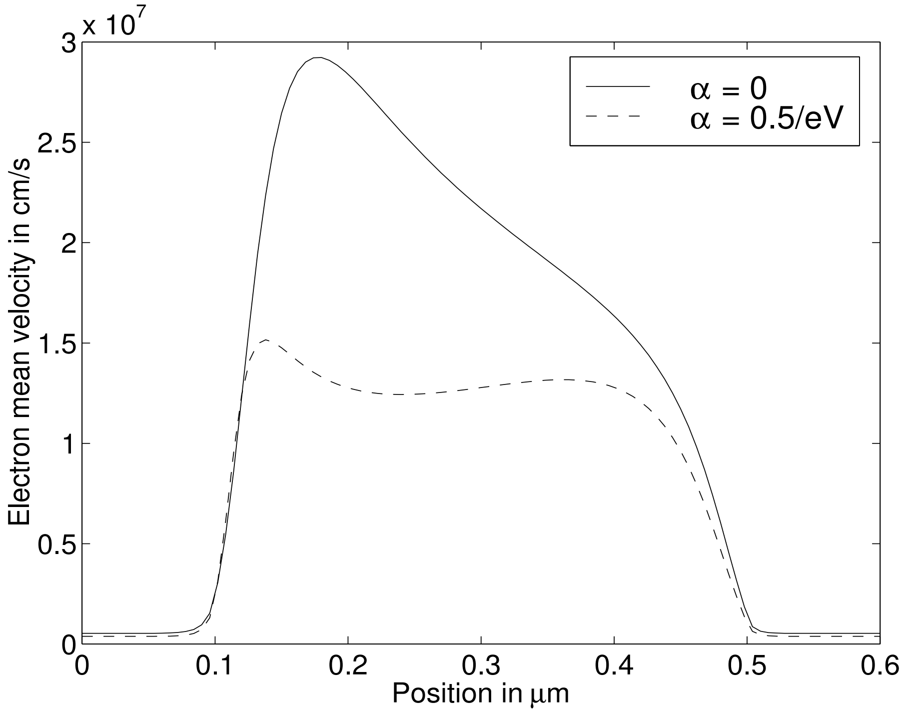

Figure 4: Electron mean velocity versus position in a ballistic diode using Lyumkis' model.

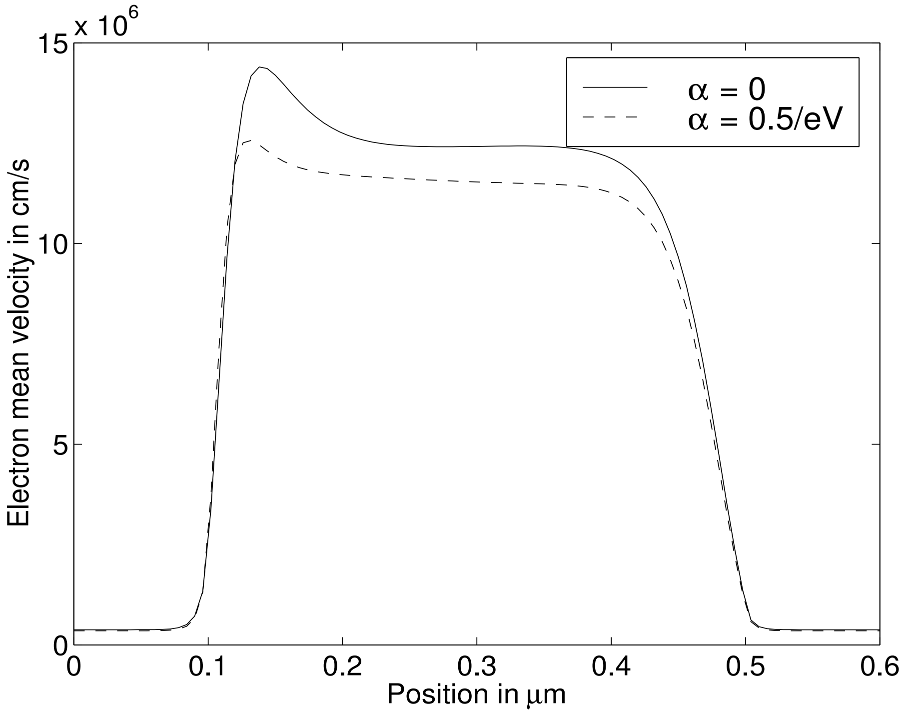

Figure 5: Electron mean velocity versus position in a ballistic diode using Chen's model.

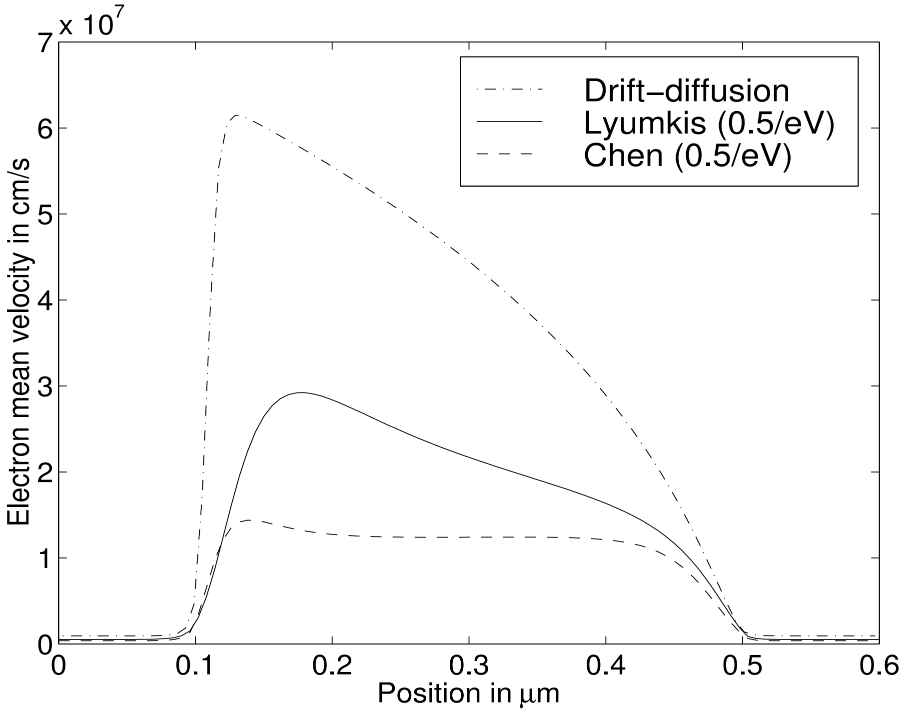

Figure 6: Electron mean velocity versus position in a ballistic diode.

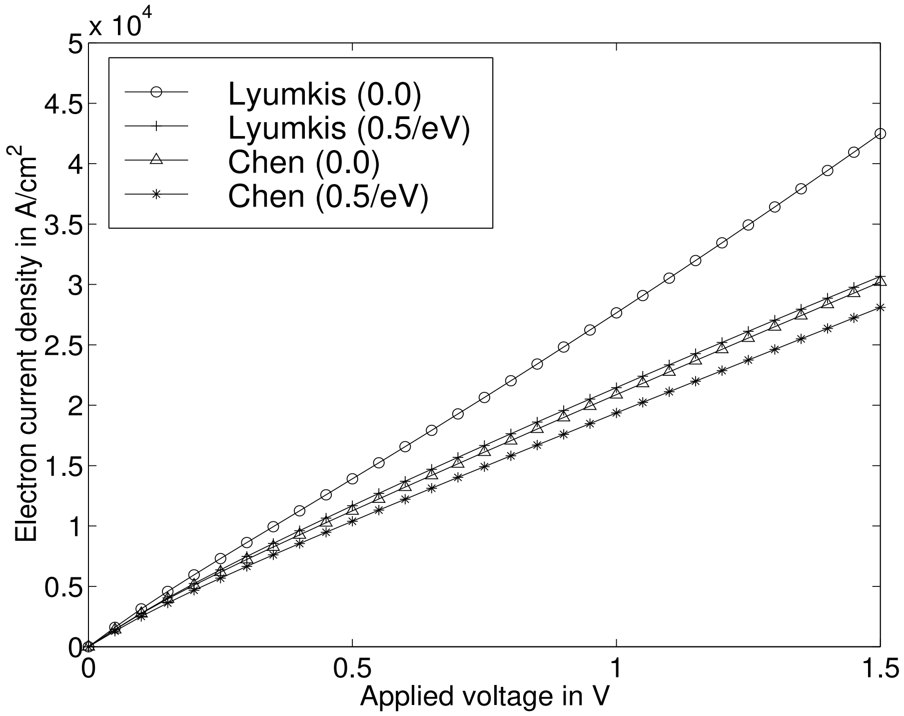

Figure 7: Current-voltage characteristics for a ballistic diode.